ACS APPLIED MATERIALS & INTERFACES

Research Article

www.acsami.org

Surface Charge-Switchable Polymeric Magnetic Nanoparticles for the Controlled Release of Anticancer Drug

Jian-Min Shen,*[,†,‡] Tao Yin,[‡,§] Xiao-Zhu Tian,[†] Fei-Yun Gao,[∥] and Shuang Xu[⊥]

[†]Department of Biochemistry and Molecular Biology, School of Life Sciences, Lanzhou University, Lanzhou, Gansu 730000, China

[‡]Key Laboratory for Magnetism and Magnetic Materials of the Ministry of Education, Lanzhou University, Lanzhou 730000, China

[§]School of Physical Science and Technology, Lanzhou University, Lanzhou 730000, China

[∥]School of Basic Medical Sciences, Lanzhou University, Lanzhou 730000, China

[⊥]College of Chemistry and Chemical Engineering, Lanzhou University, Lanzhou 730000, China

Supporting Information

ABSTRACT: We develop paclitaxel (PTX) and magnetic nanoparticles (MNPs) coencapsulated, surface charge-switchable, thermosensitive poly(D,L-lactic-co-glycolic acid)-L-lysine-D-galactose (PTX-MNP-PLGA-Lys-Gal) NPs for the controlled release of the anticancer drug. The novel dual signal-responsive nanovehicle is formulated to shield off target at pH 7.4 but bind avidly to tumor cells in acidity, alleviating toxicity and side effects of the drug to normal tissues. The mechanism involves pH-sensitive NPs surface charge switching by the deblocking process of galactose molecules followed by protonation of ε-NH_2 in lysine residue at acidic pH. Magnetic hyperthermia under near infrared (NIR) irradiation induced the contraction of PTX-MNP-PLGA-Lys-Gal NPs and, in turn, triggered burst release of PTX. Transmission electron microscopy (TEM), fluorescence microscope analyses, Fourier transform infrared (FTIR), X-ray diffraction (XRD), vibrating sample magnetometer (VSM), dynamic light scattering (DLS), and ξ-potential analyses were performed to characterize physicochemical properties of the as-prepared NPs. The size range of the globule PTX-MNP-PLGA-Lys-Gal NPs after being prescreened was from 130 to 150 nm under simulated physiological medium. The high encapsulation efficiencies of MNPs and PTX were obtained, reaching 85 and 78 wt % for PTX-MNP-PLGA-Lys-Gal NPs, respectively. The tumor inhibitory rate of 78.8% reflected that the resulting NPs could be promising to treat cancer by specific binding and targeting release drug to tumor.

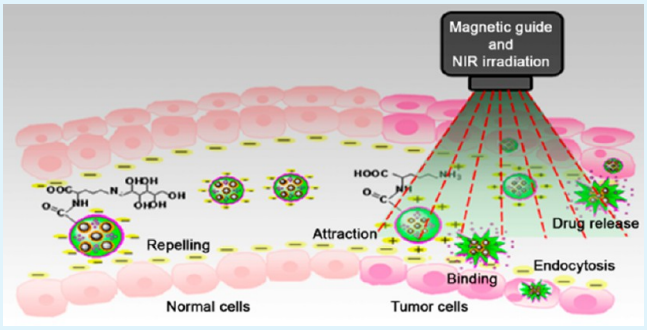

KEYWORDS: *anticancer, magnetic nanoparticles (MNPs), surface charge switching, hyperthermia, controlled release, near-infrared radiation (NIR)*

INTRODUCTION

The main bottleneck problem of systemically administered nanoparticle-based anticancer drug delivery systems is known to be efficiently targeting and releasing cytotoxic agents to tumor site in a controlled manner.[1] The property of surface charge can be exploited to target nanoparticle to tumor tissues.[2] This mechanism of specific binding to tumors relates to electrostatic attraction between positively charged nanoparticle surfaces and negatively charged cell membranes at target sites.[3] The particle surface, however, must maintain a neutral or negatively charged off the target site to avoid nonspecific binding during circulation.[4] pH-responsive surface properties can induce charge switching under tumor microenvironments. The intelligent nanovehicles responding to physiological events, including alterations in extracellular pH and local temperature, are especially effective against tumors.[5,6] These nanocarriers can regulate particles interaction with tumor cells through dynamically switching surface charge based on changed microenvironment, which enhance therapeutic efficacy and reduce undesirable side effects.[7,8] Thus, the specific intracellular uptake can be intensified by modulating the blocking/deblocking process of nonspecific ligands (such as peptide,[7] acid anhydride,[9] and polylysine[10]). In various nanoparticle preparation protocols,[11,12] poly(lactic acid-co-glycolic acid) (PLGA) has recently found widespread use due to its biocompatibility and bioabsorbability.[13] PLGA molecules acted as agglomeration matrix contain abundant end carboxyl groups lying at the nanoparticle surface, which supplies the favorable platform for the conjugation of charge switching unit via chemical bonds. Moreover, incorporation of superparamagnetic properties into this nanoparticle provides more interesting opportunities for further enhancement of targeting efficacy compared with sole property. Preferential targeting capability of delivering nanocarrier to the desired specific location in the

Received: April 8, 2013
Accepted: July 1, 2013
Published: July 1, 2013

dx.doi.org/10.1021/am401277s | ACS Appl. Mater. Interfaces 2013, 5, 7014−7024

body under magnetic manipulation would potentially magnify chemotherapy efficacy and lessen toxicity and side effects.[14]

Apart from magnetic response, magnetic nanoparticlles (MNPs) coentrapped with drugs can play two roles, including controlled release and therapeutic effects, due to their potential in hyperthermia.[15,16] The essential mechanism involves heat induction in a controllable manner, such as near-infrared radiation (NIR).[17] When encountering the noncontact stimulus, MNPs encapsulated in nanocarriers are activated and can convert radiation energy into heat with temperatures up to 45 °C.[18] In a customary occasion, it frequently takes a few days or even months to decompose PLGA NPs,[19] which does not easily accomplish the burst release of drug. However, a leaping high temperature stimuli from magnetic heat helps to trigger drug release because PLGA molecules have a lower critical solution temperature (LCST).[20] So, magnetic hyperthermia provides an opportunity for drug release from PLGA NPs. Furthermore, tumor cells are more vulnerable to increased temperature than normal cells, leading to tumor degeneration,[21,22] which has evoked the development of MNPs-based drug delivery systems to apply to hyperthermia therapy.[23] Magnetic fluid hyperthermia depends on the potential of the thermal seeds under the external induction. A crucial issue related to hyperthermia is loading sufficient MNPs into the nanovehicle with a desired size to precisely respond to external stimulus. The hydrophilic nature of the native superparamagnetic iron oxide nanoparticles, however, not only limits the loading amount of the MNPs but also hinders the entrapment of hydrophobic drug. Even though hydrophilic MNPs were narrowly wrapped into PLGA NPs, the resulting magnetic nanocarriers have oversized particle sizes due to the inclination of MNPs agglomeration in organic solvents before emulsification.[24] So, it is necessary to chemically modify the surface of the iron oxide particles prior to emulsification to increase MNPs payload.[11] Oleic acid (OA) is usually used to precoated MNPs because its hydrophobic property makes the OA-coated MNPs easily dispersive in the organic solvents. In addition, there are two major advantages to oleic acid shell. First, the hydrophobic shell provides a reservoir to enrich the hydrophobic drug for therapeutic purposes.[25] Second, oleic acid-coated metallic oxide nanofluids can enhance thermal conductivity and maintain high thermal stability.[26]

As a result, the integration of surface charge switching and magnetic function into a single platform endows nanoparticles with multiple properties, such as dual-targeting capabilities (charge attraction and magnetic induction), controllable release, and dual-therapeutical effects (drug and hyperthermia therapy), which would be enormously beneficial for cancer nanomedicine. So far, however, to the best of our knowledge, there are no reports on the integrated applications of these multifunctional networks in cancer therapy. Here, we present novel dual signal-responsive polymeric magnetic nanoparticles fabricated by the combination of a drug-MNPs coencapsulated protocol and polymer end grafting strategy based on a nonspecific D-galactose building block as the switching unit. Subsequently, tumor growth inhibition was achieved by orderly triggering three procedures, including magnetic induction, nanoparticles specific binding, and controlled release under NIR irradiation.

EXPERIMENTAL SECTION

Reagents and Materials. Ferrous chloride tetrahydrate, ferric trichloride hexahydrate, aqueous ammonia, oleic acid, L-lysine (Lys), D-galactose (Gal), 1-ethyl-3-(3-dimethylaminopropyl) carbodiimide hydrochloride (EDC), N-hydroxysuccinimide (NHS), paclitaxel (PTX), and rhodamine B (RhB) were acquired from Sigma Aldrich (Shanghai, China). P-toluenesulfonic acid and dimethyl sulfoxide (DMSO) were provided by Gansu Yinguang Chemical Industry Co. (China). All cell lines used in experiment were acquired from the cell bank (China).

Synthesis of Oleic Acid-Modified MNPs (MNPs-OA). The superparamagnetic iron oxide nanoparticles were synthesized as described in our previous literature.[27] Briefly, two kinds of iron precursor molecules were blended by a molar ratio of 2:1 and formed an aqueous solution in 20 mL of deionized water. The solution was stirred and maintained in an oil bath at 80 °C for 20 min under nitrogen gas protection. Black ferroferric oxide was obtained by adding aqueous ammonia (12.5 mL). In order to acquire dispersive hydrophobic Fe_3O_4 MNPs well in the organic solution, the MNP surface was grafted further with 9 mL of oleic acid (OA).[28] The mixture was kept for another 20 min in the oil bath. A black magnetite gel precipitated, cooled to room temperature, and mixed with 10 mL of acetone. OA-modified MNPs were separated by magnetic decantation and washed twice with acetone to remove unbounded oleic acid under sonication. The product was dried in a freezer dryer and abbreviated to MNPs-OA.

Formulation of Polymeric Magnetic NPs. Empty MNP-PLGA NPs were formulated using single emulsion (oil in water) combined with solvent evaporation methods with some modifications.[28] In brief, 50 mg of dry MNPs-OA powder was dispersed into 2 mL of PLGA solution (50 mg/mL, in dichloromethane (DCM)). Subsequently, sonication/emulsification/solvent evaporation processes of the mixture were the same as our previous report.[29]

For the preparation of PTX-loaded MNP-PLGA, 50 mg of dry MNPs-OA powder and PTX (5 mg) were mixed into 2 mL of PLGA solution (50 mg/mL, in DCM). Other processes were the same as above. The products were denoted as PTX-MNP-PLGA NPs. PTX-unloaded content in all the supernatants was determined by ultrafiltration and a RP-HPLC method described in the Supporting Information. The loading amount of PTX in NPs was determined by subtracting uncombined PTX amount from original added amount, accordingly, the entrapment efficiency of PTX was obtained. PTX-loaded MNPs-uncontained PLGA NPs were also prepared in a similar way except omitting the addition of MNPs. The product was denoted as PTX-PLGA NPs. To observe the drug release process and determine cellular uptake by fluorescent probe, RhB-labeled MNP-PLGA NPs were prepared using a similar procedure. Typically, 100 μL of RhB solution (50 mg/mL, in DCM) was added dropwise to magnetite oily suspension prior to emulsification. Afterward, all preparations were achieved in the dark. The product was denoted as RhB-MNP-PLGA NPs.

Finally, all products were redispersed in N_2−H_2O and centrifugated at 400 rpm for 1 min to remove oversized particles. Then, supernatants were lyophilized under vacuum for three days (Huier VFD-1000, China) to get powdery NPs for further use and stored at 4 °C.

Synthesis of Lys−Gal-Conjugated Polymeric NPs. L-lysine−D-galactose Schiff base was synthesized using a previous method with some modifications.[30] In brief, L-lysine (1.46 g) and D-galactose (2.70 g) were added in 25 mL anhydrous ethanol at molar ratio of 1:1.5. After the addition of a catalyst (p-toluenesulfonic acid), the reaction mixture was refluxed for 24 h with stirring at 80 °C, followed by concentrating under vacuum. The residue was purified on a preparation column through RP-HPLC to give the product. The purified Lys−Gal compound was then lyophilized.

To conjugate Lys−Gal moiety with polymeric NPs, 150 mg of the as-prepared MNP-PLGA, PTX-MNP-PLGA, PTX-PLGA, and RhB-MNP-PLGA NPs were dispersed ultrasonically in 5 mL of N_2−H_2O. The COOH groups from PLGA molecules on NP surface were first activated by adding 30 mg NHS and 54 mg EDC. Excess NHS and EDC were removed by centrifugation. The precipitation was confected into 3 mL of suspension (in N_2−H_2O). Then, 4 aliquots of Lys−Gal solution (2 mL, 0.0165 mmol/mL) were mixed with the activated NPs

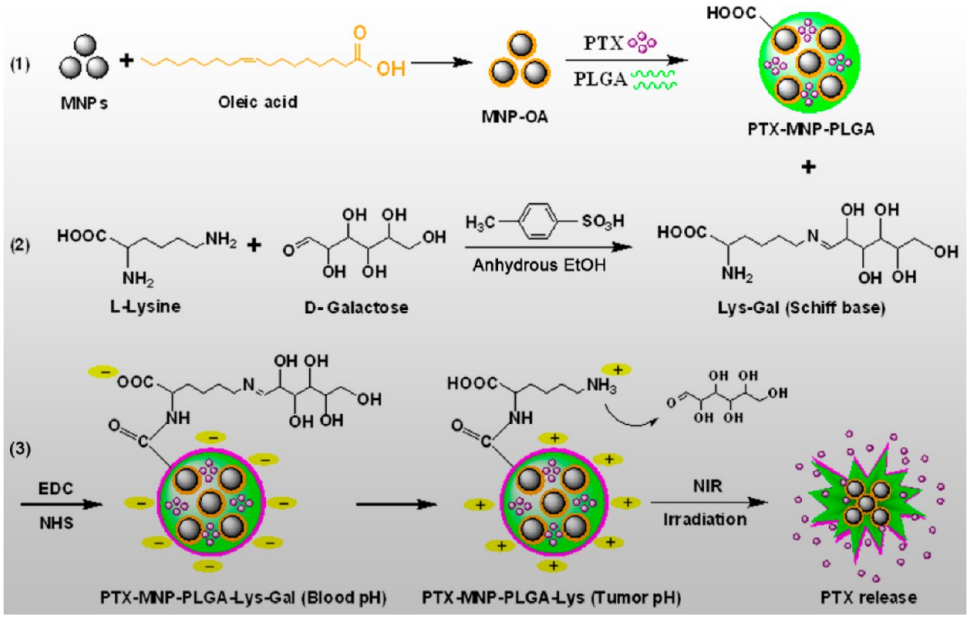

Figure 1. Schematic diagram of designing pH-switchable polymeric magnetic nanoparticles and controlled release triggered by NIR irradiation.

suspension. Shaking overnight under nitrogen protection was performed on a level swing bed. The end products were washed three times and abbreviated to MNP-PLGA-Lys-Gal, PTX-MNP-PLGA-Lys-Gal, PTX-PLGA-Lys-Gal, and RhB-MNP-PLGA-Lys-Gal NPs. Moreover, MNP-PLGA-Lys, PTX-MNP-PLGA-Lys, and RhB-MNP-PLGA-Lys NPs were also prepared by conjugating directly L-lysine to their precursors under the activation of NHS and EDC in order to compare pH-switchable NPs with pH-unswitchable NPs in properties, such as specificity, biocompatibility, and anticancer activity.

Physicochemical Property Characterization. The NP morphology was examined by transmission electron microscopy (TEM, TecnaiG^2 F30, FEI, U.S.A.), fluorescence microscope (Nikon TE2000-S, Japan), and an optical microscope (Motic, BA 200, China). Large-angle (10∼80°) powder XRD spectra were recorded to determine the existence of magnetic crystallographic composition in NPs by Cu Kα radiation at X'Pert PRO (PANalytical, Holand). Mass spectrometer assay was achieved on a Bruker spectrometer (Maxis 4G, U.S.A.). Fourier transform infrared (FTIR) spectra were obtained on an FTIR spectrometer (Nicolet, U.S.A.). The MNPs content in resulting NPs was assayed by thermogravimetric analysis (TGA, Diamond TG/DTA6300, Perkin-Elmer, U.S.A.) under nitrogen gas protection. The magnetization of dried products (about 12 mg) were measured on vibrating sample magnetometer (VSM) (Lake Shore, U.S.A.). The ζ-potentials of NPs (500 μg/mL) at different pH (pH 7.5−5.0) and different media (PBS or HSA-containing PBS) were recorded on a Zetasizer (Nano 3600, Malvern, U.K.) in triplicate. The hydrodynamic sizes of the different products in PBS medium (50 mM, pH 7.4) were tested by a BI-200SM DLS (Brookhaven, U.S.A.) with angle detection at 90°.

In Vitro NIR-Triggered Drug Release. Initially, inductive heating experiments were conducted by NIR irradiation in order to ascertain inductive heating ability from MNPs. 100 mg of the lyophilized PTX-MNP-PLGA-Lys-Gal and PTX-PLGA-Lys-Gal powders were prepared into 10 mL of suspension in an ampule bottle (in 50 mM PBS, pH 7.4), respectively. The temperature was measured accurately at defined time points using a mercurial thermometer in suspension about 10 cm from the NIR irradiation source (2W). At the same time, the degradation rates of the PTX-MNP-PLGA-Lys-Gal NPs both in the presence and absence of NIR were also researched. Subsequently, the release of PTX from the PTX-MNP-PLGA-Lys-Gal or PTX-PLGA-Lys-Gal NPs was triggered by NIR irradiation externally to explore the interrelation between heat conduction and drug release in neutral or acidic media (50 mM PBS, pH 7.4, and pH 5.3). Similar operation has been described in our previous work.[29] Briefly, 100 mg of the lyophilized PTX-MNP-PLGA-Lys-Gal or PTX-PLGA-Lys-Gal powder was placed in an ampule bottle and dispersed in 10 mL of PBS. Then, the different suspensions were kept at 20 °C in a thermostat for 5 min to stabilize the system and irradiated using the near-infrared ray. The absorbance of PTX released into the PBS was assayed by UV−visible spectrophotometer (ThermoFisher Evolution 300, China) at 277 nm at defined time points.

In Vitro Cell Uptake Imaging. A549 cells and CCL-171 cells were grown on a 6-well plate (6×10^4 cells/well) at 37 °C for 24 h. When the cell culture reached about 80% confluence, RhB-MNP-PLGA-Lys and RhB-MNP-PLGA-Lys-Gal NPs suspensions (200 μg/mL) were added, respectively. After being incubated for another 2 h at 37 °C, the cells were rinsed carefully three times with ice-cold PBS (1 mL) to remove the unbound NPs, followed by fixation with 4% paraformaldehyde (0.5 mL) for 20 min. The cellular uptake was visualized by LSCM (ZEISS, 510 Meta, Germany) under excitation wavelength of 514 nm.

In Vitro Cytotoxicity. The cytotoxicity of the NPs was analyzed using the MTT method. The similar methods have been presented in our publication.[29,31] In the present work, A549 cells and CCL-171 cells were cultured in a 96-well plate at a density of 1×10^4 cells per well in lysine-free RPMI-1640 medium supplemented with 10% fetal calf serum and 1% penicillin/streptomycin at 37 °C with 5% CO_2 for 24 h. The cells were then treated with the four types of NPs (MNP-PLGA-Lys-Gal, PTX-MNP-PLGA-Lys-Gal, MNP-PLGA-Lys, and PTX-MNP-PLGA-Lys) with a concentration from 5 to 640 μg/mL for another 24 h, respectively. The subsequent operations were the same as the literature.[29,31]

Hemolysis Analysis In Vitro. The preparation and dilution of human red blood cells (HRBCs) were described in our previous protocol.[31] Then, the analysis included two groups: PTX-MNP-PLGA-Lys and PTX-MNP-PLGA-Lys-Gal NPs. The every group was again divided into three sections, and 8 aliquots of 0.1 mL of the diluted HRBC suspension mixed with 1.9 mL of NPs at concentrations of 10, 50, 100, 200, 400, 600, 800, and 1000 μg/mL. Hemolysis caused by PBS (50 mM, pH 7.4) and deionized water were used as negative and positive control, respectively. The subsequent operation and calculation of hemolysis percentages were the same as in our previously published articles.[31]

Magnetic Guide and Drug-Coupled NIR Treatment Vivo. To compare the therapeutic efficacies of PTX-PLGA-Lys-Gal, PTX-MNP-PLGA-Lys, and PTX-MNP-PLGA-Lys-Gal NPs in tumor inhibition application, the female sarcoma 180-bearing Balb/c mice model (body weight 18−22 g) was built by subcutaneous transplantation of 2×10^6

sarcoma-180 ascites tumor cells (0.2 mL) into the right front oxter region. The welfare and experimental procedures of mice were described in our previous protocol.[29] On day 6 after tumor cell inoculation, the mice were treated with different NPs suspension in sterile PBS irradiated by ^{60}Co by tail vein (n = 5/group, 0.2 mL per mouse, 2 mg/kg body weight) every other day for 14 days, respectively. NPs included PTX-PLGA-Lys-Gal, PTX-MNP-PLGA-Lys, and PTX-MNP-PLGA-Lys-Gal). The control group mice were given 0.2 mL of sterile PBS at the same way on the same schedule. As soon as the injection was performed, the mice were anesthetized using isoflurane and settled down. After induced for 3 h with a constant magnet field at 25 °C, the inoculation site was treated using a 10 mm laser spot (2 W) for 20 min. According to the description of our previous literature,[29] on day 14, all the mice were sacrificed and the tumor inhibition rate was determined.[32]

Biodistribution Patterns In Vivo. In order to determine distribution of PTX in various tissues, another 20 male S-180 sarcoma-bearing Balb/c mice were anesthetized by intraperitoneally injecting 20% chloral hydrate. Then, 0.2 mL of the PTX-PLGA-Lys-Gal, PTX-MNP-PLGA-Lys, and PTX-MNP-PLGA-Lys-Gal NP suspension were injected as mentioned above. The PTX group was given 0.2 mL of free PTX solution (in sterile PBS) corresponding to the PTX content uploaded in NPs. The magnetic guide and treatment procedure in vivo were performed. The extraction and preparation of PTX from plasma and six tissues, such as heart, liver, spleen, lung, kidney and tumor, were the same as that of DOX in our previous report.[29] Then, the PTX-containing samples were analyzed based on RP-HPLC. The method of PTX quantification can be seen in the Supporting Information. Representative chromatograms of PTX are presented in Figure S1.

RESULTS AND DISCUSSION

Synthesis of the PTX-MNP-PLGA-Lys-Gal NPs. Ingredients used for NPs formulation, such as MNPs, PLGA, PVA, Lys, and Gal, present biocompatibility. Synthesis of the PTX-MNP-PLGA-Lys-Gal NPs included three aspects. First, it is necessary to coat the resultant MNPs using oleic acid (OA) to obtain dispersive hydrophobic MNP-OA NPs and enhance thermal conductivity of subsequent polymeric magnetic NPs. Then, OA-coated MNPs together with anticancer PTX were encapsulated and distributed in PLGA nanoparticles (Figure 1(1)). Second, the Schiff-base amino alcohols (Lys−Gal) were prepared from L-lysine and D-galactose in only one step with overall yields of up to 76% (Figure 1(2)). In the reaction, p-toluenesulfonic acid served as a catalyst, and anhydrous EtOH was used as solvent and water absorbent where two precursors were not dissolved for easy separation of product. Third, the pH-switchable polymeric magnetic NPs were fabricated by formation of amide bond between the carboxyl groups of PLGA and ε-NH_2 of lysine residues from Lys−Gal (Figure 1(3)).

Characterization of the PTX-MNP-PLGA-Lys-Gal NPs. Figure 2 shows the morphology of the resulting NPs taken by transmission electron microscope (TEM), fluorescence microscope, and optical microscope. According to the TEM images, the dispersive OA-coated MNPs were obtained (Figure 2A), and the synthesized PTX-MNP-PLGA-Lys-Gal NPs tended to be dispersive and sphere with the particle sizes about 130 nm (Figure 2B). The TEM image showed that the MNP-OA NPs were randomly scattered within the nanoparticle. It can be found from the fluorescence and optical microscope images that RhB-labeled PTX-MNP-PLGA-Lys-Gal NPs have a slightly increased particle sizes (about average 140 nm, Figure 2C, D). It is clear that there are many MNPs (black shadow) uniformly dispersed in the PLGA matrix (Figure 2C).

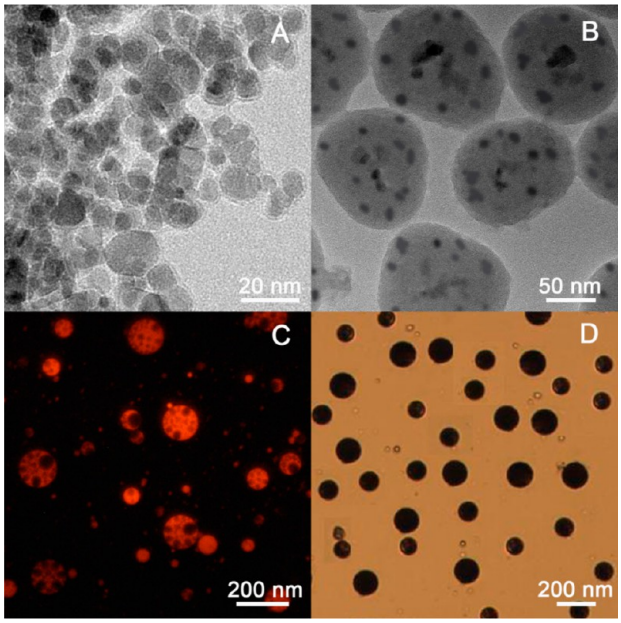

Figure 2. (A and B) TEM images of oleic acid-coated MNPs and PTX-MNP-PLGA-Lys-Gal NP. (C and D) Fluorescence and optical microscope images of the resulting RhB-labeled PTX-MNP-PLGA-Lys-Gal NPs. Fluorescent excitation wavelength = 514 nm.

Based on XRD profiles, the intensities of characteristic peaks (111, 220, 311, 400, 422, 440) of magnetite nanoparticles from PTX-MNP-PLGA-Lys-Gal NPs (Figure 3A(c)) were weaker than those from PTX-MNP-PLGA (Figure 3A(b)) and MNPs-OA (Figure 3A(a)) in proper sequence, indicating the gradual introduction of amorphous materials (PTX, PLGA, PVA, and Lys−Gal) on the MNP-OA NPs surface. Figure 3B shows mass spectrum of the resulting Lys−Gal Schiff base with a molecular weight of 309.18.

The FTIR spectra of the MNP-OA (Figure 3C(a)) presented the special peak at 590 cm^{-1} related to Fe_3O_4, a peak of hydroxy group at 3400 cm^{-1}, two sharp peaks of methylene group at 2900 cm^{-1} and 2850 cm^{-1}, a peak of carbonyl group at 1700 cm^{-1}, and a peak of cis-alkene at 960 cm^{-1}. All these results showed MNPs have been expectably coated by oleic acid. Two peaks of hydroxy groups at 3400 cm^{-1} and 1060 cm^{-1}, and C−O stretching got stronger in the PTX-MNP-PLGA (Figure 3C(b)) compared with those of MNP-OA, and a peak corresponding to C═O was red-shifted from 1700 cm^{-1} into 1750 cm^{-1}, reflecting that more hydroxy groups deriving from PTX and PLGA were loaded onto the NPs. Moreover, two new characteristic peaks appeared at 1600 cm^{-1} and 1500 cm^{-1}, indicating the introduction of the benzene rings deriving from PTX molecule. In the case of PTX-MNP-PLGA-Lys-Gal (Figure 3C(c)), two new characteristic peaks appeared at 1620 cm^{-1} and 1200 cm^{-1} related to the N−H vibration of tert-amino group and C−N vibration of cyanogroup, respectively, demonstrating the introduction of the Schiff base. Furthermore, an absorption peak of C═O and $CONH_2$ groups deriving from Schiff base at 1750 cm^{-1} was also stronger than those of MNP-OA and PTX-MNP-PLGA NPs, verifying forcefully fabrication of Lys−Gal moiety on PTX-MNP-PLGA NPs.

Figure 3D indicates mass loss of the different compounds under high temperature. A 9.7% mass decrease of MNP-OA at 800 °C demonstrated the successful coating of OA. A 49% mass decline of PTX-MNP-PLGA at 800 °C suggested that the

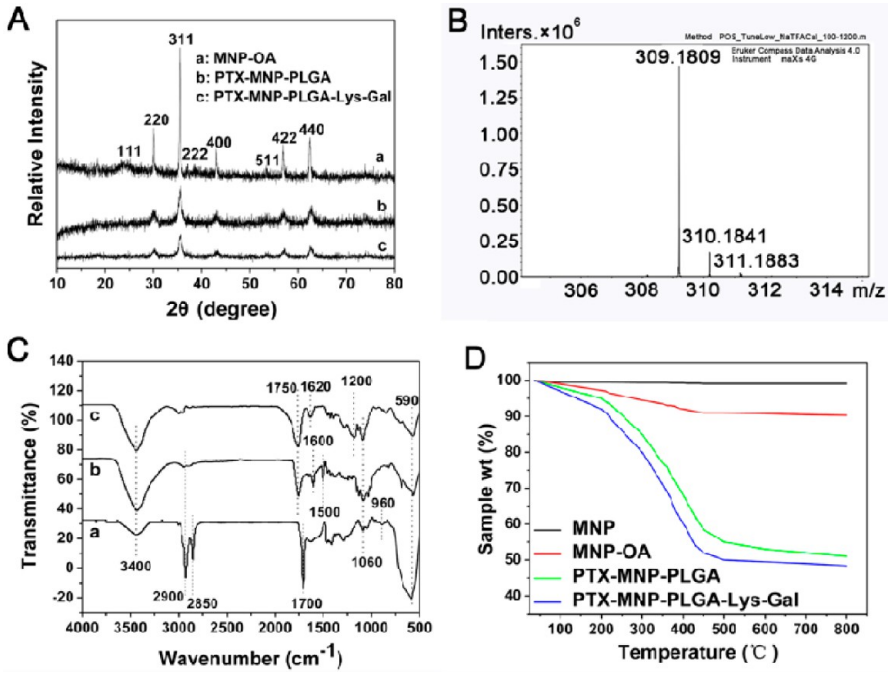

Figure 3. (A) XRD patterns of MNP-OA, PTX-MNP-PLGA, and PTX-MNP-PLGA-Lys-Gal NPs. (B) Mass spectrum of the resulting Lys−Gal Schiff base. (C) FTIR spectra of (a) MNP-OA, (b) PTX-MNP-PLGA, (c) PTX-MNP-PLGA-Lys-Gal NPs. (D) Thermogravimetric assay (TGA) of the different nanoparticles.

MNPs accounted for 51% of the compound. Moreover, a 2.6% mass decrease existed in end product PTX-MNP-PLGA-Lys-Gal compared with PTX-MNP-PLGA at 800 °C. These results plainly confirmed that the resulting PTX-MNP-PLGA-Lys-Gal NPs were composed of abundant MNPs and PLGA, and a small number of PTX and Lys−Gal Schiff base by mass.

It can be found from the VSM magnetization properties (Figure 4A), that although the saturation magnetization intensity gradually weakened with the increase of the shell thickness of NPs, the saturation magnetization of the end product PTX-MNP-PLGA-Lys-Gal NPs (about 44.6 emu/g) still reached approximately 55.1% of that of the MNPs-OA (80.9 emu/g). This will provide a sufficient magnetic responsiveness and thermal conductivity for the use for magnetic manipulation and hyperthermia. To obtain the uniform PTX-MNP-PLGA-Lys-Gal NPs, the synthesized NPs were prescreened to remove oversized particles using the centrifugation method at low speed, which can avoid capillary blockage and being intercepted by endomembrane system during circulation. The average size of PTX-MNP-PLGA-Lys-Gal reached 139 nm (Table 1) based on DLS. The datum was slightly bigger than that obtained by TEM due to hydrodynamic dispersion. Furthermore, there was no change in particle size for the NPs over a period of 5 days (data not shown), indicating no occurrence of NPs aggregation in the meanwhile.

Encapsulation Efficiencies of MNPs and PTX. The encapsulation efficiencies of MNPs and PTX accounted for 85 wt % (283 mg/g) and 78 wt % (26 mg/g) for PTX-MNP-PLGA (OA-containing system), respectively (Table 1). In the absence of the oleic acid system, however, the encapsulation efficiencies of MNPs and PTX were merely 37 wt % (123 mg/g) and 24 wt % (8 mg/g), respectively. Apparently, in the presence of oleic acid, the encapsulation efficiencies of MNPs and PTX presented approximately 2.3-fold and 3.3-fold increases, respectively. Furthermore, the loading of PTX also displayed a similar situation in MNPs-unentrapped PTX-PLGA-Lys-Gal NPs, where encapsulation efficiency of PTX was only 22 wt %.

On the one hand, due to the hydrophilic nature of the native superparamagnetic iron oxide nanoparticles, the MNPs are inclined to agglomeration in organic solvents.[24] During encapsulation of MNPs along with hydrophobic drug into NPs, the MNPs tend to be excluded. In the present work, oleic acid gets chemisorbed on the surface of the iron oxide particles. The hydrophobic property of the oleic acid makes the OA-coated MNPs uniformly dispersive in the organic solvents and easily coated by PLGA. In addition, with the modification of OA on MNPs surface, hydrophobic PTX was subject to affinity attraction of OA in the emulsifying process of oil/water.

On the other hand, the heating of the local tissue depends on the specific absorption rate, which is defined as the capability that radiant energy is absorbed by a unit mass of a biological material.[22] Generally speaking, the more the MNPs are entrapped into NPs, the higher the heat generates. Moreover, the saturation magnetization of the as-prepared NPs also relies on the loading amount of the MNPs to a large extent. Thus, the encapsulation effciency of MNPs in NPs is a main parameter determining the hyperthermia level and magnetic responsiveness.

pH-Triggered Surface Charge Switching. The kinetics of the pH-responsive property of the PTX-MNP-PLGA-Lys-Gal NPs surface was evaluated over time in PBS at 37 °C by the ζ-potential measurement (Figure 4B). Taking data at 4 h as an example, in the present experimental condition, as the pH of the NPs solution reduced from pH 7.5 to 5.0, the ζ-potential of the NPs increased from −13.8 to +31 mV, deducing the removal of galactose from Schiff base. This particulate system designed for targeting to tumor may switch the surface charge of the PTX-MNP-PLGA-Lys-Gal NPs from anionic above pH

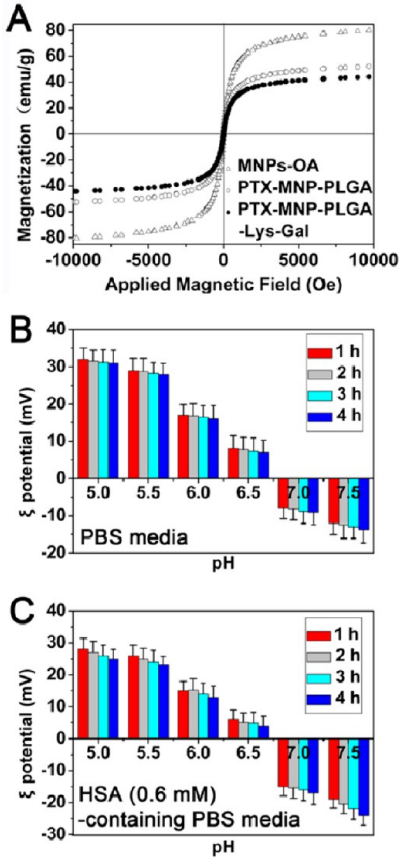

Figure 4. (A) VSM curves of the different NPs at 305 K. (B and C) ζ-Potential charges (n = 3) of PTX-MNP-PLGA-Lys-Gal NPs in PBS and HSA (0.6 mM)-containing PBS media at different pH values. The NPs in solution (500 μg/mL, 50 mM PBS) at each pH was maintained for 1, 2, 3, and 4 h at 37 °C. All NPs were stabilized at each pH for 10 min prior to measuring the ζ-potential.

Table 1. Physical Properties of the Different Nanoparticles

nanoparticles	particle size[a] (nm ± SD)	encapsulation efficiency of MNPs[b] (%) ± SD	encapsulation efficiency of PTX[c] (%) ± SD
MNP-OA	13 ± 1.1		
PTX-MNP-PLGA	133 ± 6.3	85 ± 3.4	78 ± 4.6
PTX-MNP-PLGA-Lys-Gal	139 ± 5.9	85 ± 3.4	78 ± 4.6
RhB-labeled PTX-MNP-PLGA-Lys-Gal	141 ± 4.5	85 ± 3.4	78 ± 4.6
PTX-MNP-PLGA (free OA)	101 ± 4.2	37 ± 1.6	24 ± 3.1
PTX-PLGA-Lys-Gal	33 ± 2.8		22 ± 3.6

[a]Particle size was detected by DLS. [b]Encapsulation efficiency of MNPs was determined by TGA. [c]Encapsulation efficiency of PTX was assayed by RP-HPLC.

7.0 to cationic below pH 6.5. Furthermore, the lower the pH of the NPs solution was, the more the galactose was chemically dissociated, in turn, the higher protonation degree of ε-NH_2 in lysine residue was. The ζ-potential of the NPs around pH 5.0–5.5 displayed the maximum value in test pH (Figure 4B), implying that the surface charge of PTX-MNP-PLGA-Lys-Gal NPs may be switchable under tumor microenvironment pH by the deblocking process of galactose molecules. With respect to the ζ-potential at other point in time at various pH values, the trend of data is consistent with that at 4 h.

In view of the NPs-protein adsorption that can to some extent affect charge properties of NPs in serum, it is necessary to measure ζ-potential in a serum protein-containing media. As is well-known, albumin is the most abundant protein that contents generally a concentration of 0.6 mM.[33] So, this experiment is done in a HSA (0.6 mM)-containing PBS media. The results show that, as compared in HSA-containing PBS media with in PBS, within pH 5.0–6.5 range, the ζ-potential of NPs is slightly lower, when above pH 7, the absolute values of the ζ-potential of NPs are higher (Figure 4C). We deduce that this may be attributed to the solubility of HSA in various media. When at pH 5.0, the solubility of HSA is relatively low because the pH value is close to its isoelectric point (pI = 4.7); so, the aggregating HSA is in favor of attracting with NPs, which leads to the decrease of net positive charge of free NPs. The total charge, however, is still positive, indicating that NPs are still apt to bind to tumor cells in an acidic microenvironment. With the pH increase, especially, when above pH 7, the solubility of HSA is relatively high, and the negatively charged HSA molecules are unfavorable to bind with negatively charged NPs, and accordingly, the net negative charge of free NPs would increase. This effect is more and more obvious as time increases from 1 to 4 h. This is exactly what we expect; that is, NPs could principally be distributed around tumor tissues rather than located in that normal section. Thus, the PTX-MNP-PLGA-Lys-Gal NPs may hold a promise as a pH-regulated targeting delivery vehicle for potential cancer therapy.

pH-Responsive NIR-Triggered PTX Release In Vitro. In this section, the following four aspects were highlighted: (1) determination of inductive heating ability from MNPs, (2) assay of degradation rates of the NPs both in the presence and absence of NIR, (3) pH-responsive NIR-triggered drug release, and (4) dynamical observation of the RhB-labeled MNP-PLGA-Lys-Gal NPs morphology under NIR irradiation.

Figure 5A shows the results of inductive heating of the PTX-MNP-PLGA-Lys-Gal and PTX-PLGA-Lys-Gal NPs, where the temperature was measured by a mercurial thermometer in an aqueous NPs suspension. Temperature increased to 52.5 °C for the PTX-MNP-PLGA-Lys-Gal NPs under NIR irradiation (808 ± 3 nm) with power ca. 2 W/cm^2 for 10 min, while PTX-PLGA-Lys-Gal NPs only reached 29 °C. When irradiating for 30 min, temperature increased to 58 °C for the former, while the latter only reached 33 °C. Inductive heating presents in the form of thermal energy induced from the hysteresis loss of ferrites. Magnetic fluid hyperthermia depends on the potential of the thermal seeds in remagnetization process under the NIR irradiation. According to the magnetic heating mechanism,[34] the energy absorption of ferrofluids is related to the size of the superparamagnetic crystals. In the resulting PTX-MNP-PLGA-Lys-Gal NPs, the size of entrapped MNPs was about 10–12 nm, which met the requirement of magnetic relaxation of ferrofluids.[34] Oleic acid-coated metallic oxide nanofluids, furthermore, can enhance thermal conductivity and maintain high thermal stability.[24] These results indicated that, under the given NIR irradiation parameters (808 ± 3 nm diode laser, 2W), abundant energy accumulation was obtained and the temperature was drastically elevated to 58 °C for the PTX-MNP-PLGA-Lys-Gal NPs suspension (100 mg samples in 10 mL of PBS in a transparent vial) in a short time. This temperature was approximately 1.76 times higher than that of the MNPs-uncontaining PTX-PLGA-Lys-Gal NPs (33 °C),

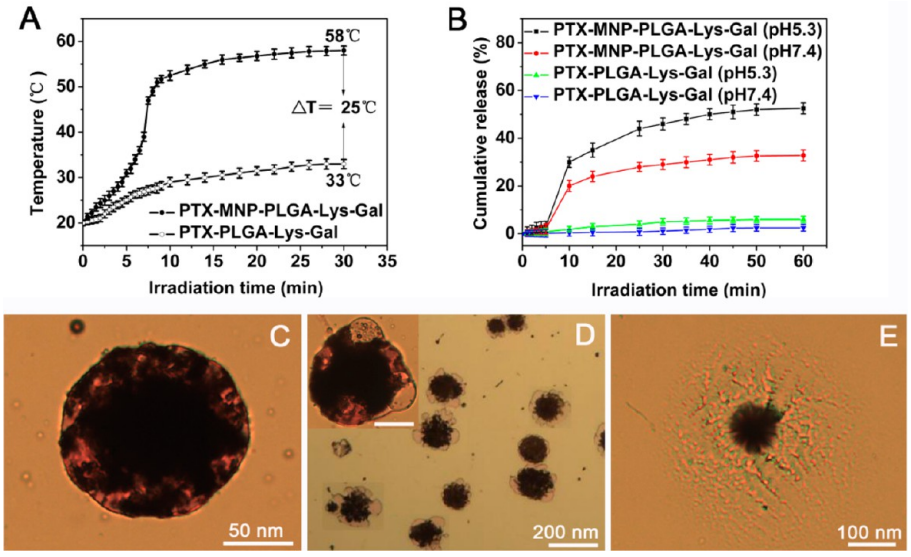

Figure 5. (A) Inductive heating experiments in PBS (50 mM, pH 7.4) under NIR irradiation. (B) In vitro release profiles of PTX from PTX-MNP-PLGA-Lys-Gal and PTX-PLGA-Lys-Gal NPs in PBS (pH 5.3 and pH 7.4) under NIR irradiation at various time points. (C–E) The optical microscope images of the RhB-labeled MNP-PLGA-Lys-Gal NPs after NIR irradiation (808 ± 3 nm) with power ca. 2 W/cm^2 for 0 min (C), 7.5 min (inset in D, the scale bar shows 50 nm), 15 min (D), and 20 min (E) in PBS (50 mM, pH 5.3).

reflecting that the difference in temperature (ΔT = 25 °C) was only attributed to the inductive heating effect of the MNPs under NIR irradiation. So, when the PTX-MNP-PLGA-Lys-Gal NPs were radiated for 10 min under NIR, the magnetic hyperthermia generated could lead to the rupture of PLGA nanoparticle because the temperature was located over the scope of lower critical solution temperature (LCST = 42–45 °C) of PLGA. Furthermore, the degradation rates of the nanoparticles both in the presence and absence of NIR have also been presented in the Supporting Information file (Table S1). Obviously, in the presence of NIR, the degradation rate of the PTX-MNP-PLGA-Lys-Gal NPs is much higher than that in the absence of NIR. Accordingly, the controlled drug release can be achieved by the application of NIR.

Drug release patterns were estimated on NIR irradiation occasions in two kinds of simulative physiological environments. As shown in Figure 5B, for the first 5 min of the exposure to NIR beam, all test NPs displayed a low cumulative release percent (below 3%), which was due to insufficient heat. In the case of PTX-PLGA-Lys-Gal NPs, the cumulative release only reached 6% at pH 5.3 and 2.5% at pH 7.4, respectively, even though the release continued for 60 min under NIR irradiation, which was attributed to the absence of heating seeds (MNPs). However, the first burst release of PTX from PTX-MNP-PLGA-Lys-Gal NPs was clearly demonstrated when NPs were radiated for 10 min by NIR, where temperature was over LCST of PLGA (Figure 5A), the release percent of PTX at pH 5.3, in particular, increased sharply from 3% at 5 min to 30% at 10 min. Subsequently, the second burst release of PTX from PTX-MNP-PLGA-Lys-Gal was observed during 10–30 min at pH 5.3, while release at pH 7.4 maintained a relatively stable rate. The increased release percent with the prolonging of the NIR irradiation time may be attributed to the volume shrinkage of the PLGA shell layer due to magnetic hyperthermia; in turn, PTX was elbowed out. In addition, the release efficiency of PTX from the NPs, whether in the presence of MNPs or in the absence, was higher under acidic conditions than neutral conditions (Figure 5B). This may be because the ester bonds of PLGA molecules were susceptible to low pH medium,[35] leading to quick degeneration of PLGA and escape of PTX. Another possible reason may be that, at pH 5.3, galactose tended to fall off from the Schiff base conjugated onto NPs, which made shell degraded and more drug was released. As expected, the pH-sensitive release pattern contributes to targeting release of PTX in tumor microenvironment (acidic environment).

In order to observe the release processes of drug from the NPs, the morphology of the RhB-labeled MNP-PLGA-Lys-Gal NPs was recorded dynamically under NIR irradiation in PBS (50 mM, pH 5.3) (Figure 5C–E). As shown in Figure 5C, all over the polymer matrix in NPs revealed bright red RhB moiety besides black MNPs. When induced by NIR irradiation, RhB-MNP-PLGA-Lys-Gal NPs showed bulliform surface protuberances at 7.5 min (inset in D) and flower-like protuberances at 15 min (Figure 5D), and the color at protuberance sites became light, showing the release of RhB. Furthermore, it is very clear that the particles size degraded into less than 100 nm after NIR irradiation for 20 min, and there is a circle of heavy red secretion around residue core (Figure 5E), suggesting that the shrinkage of RhB-MNP-PLGA-Lys-Gal NPs caused the outleaking of entrapped RhB molecules from NPs.

In Vitro Cellular Uptake Imaging. In vitro cellular uptake was assessed by laser scanning confocal microscopy (LSCM). In order to eliminate possible fluorescence interference from PTX, empty RhB-labeled NPs were used to research cellular uptake. From LSCM images of A549 cells treated with the two RhB-labeled NPs (200 μg/mL) for 2 h, it can be observed that the amount of scattering RhB-MNP-PLGA-Lys NPs (Figure 6A) was significant higher than that of RhB-MNP-PLGA-Lys-Gal (Figure 6B) within the A549 cells under identical condition. In addition, more diffuse fluorescence from RhB-MNP-PLGA-Lys NPs was found (Figure 6A) compared with RhB-MNP-PLGA-Lys-Gal NPs where fluorescence was more punctuate (Figure 6B). This further verifies the mechanism that exposed lysine residues enhanced the endocytosis of the NPs due to electrostatic attraction when compared to NPs blocked by galactose. In order to compare cancer cellular uptake with normal cells, CCL-171 cellular uptake imaging (Figure 6C, D) was also conducted. We can clearly observe significantly better

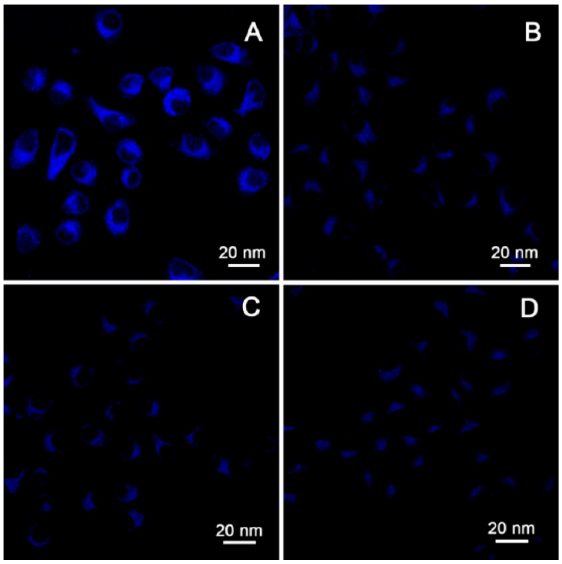

Figure 6. LSCM images of representative A549 cells and CCL-171 cells treated with the two types of RhB-labeled NPs (200 μg/mL). (A) A549 cells + RhB-MNP-PLGA-Lys, (B) A549 cells + RhB-MNP-PLGA-Lys-Gal, (C) CCL-171 cells + RhB-MNP-PLGA-Lys, (D) CCL-171 cells + RhB-MNP-PLGA-Lys-Gal. Excitation laser wavelength = 514 nm.

cellular uptake from cancer cell than normal cell for particles (Figure 6 A, B vs C, D).

Cytotoxicity In Vitro. Human lung cancer A549 cell line and human normal CCL-171 cell line were used to incubate with empty or PTX-loaded MNP-PLGA-Lys-Gal and MNP-PLGA-Lys NPs. As shown in Figure 7A, in the case of empty NPs, the triblock (PLGA-Lys-Gal) NPs revealed higher cell viability (89%) for A549 cells than diblock (PLGA-Lys) NPs (78%) at 640 μg/mL, indicating that the latter caused more serious damage to cell than the former because cationic surfaces introduced by lysine residues are more likely to bind to negatively charged cell membranes. In the case of MNP-PLGA-Lys-Gal NPs, however, cations were shielded by galactose in the Schiff base. As a result, the electrostatic attraction of the formed triblock NPs to cell membrane reduced. These cytotoxicity results also showed that the empty NPs possessed higher biocompatibility in comparison with cRGD-functionalized polymeric magnetic nanoparticles synthesized in our previous work,[29] where empty NPs had a cell viability above 70% to S-180 cells at a concentration of 320 μg/mL.

Furthermore, it can be found that PTX-loaded NPs always held higher growth inhibitory property for cancer cell than empty NPs no matter in the triblock or diblock. 82% and 55% of viabilities in A549 cells were watched at a PTX-MNP-PLGA-Lys-Gal or PTX-MNP-PLGA-Lys NPs concentration of 640 μg/mL, respectively, while 89% and 78% of viabilities were presented in A549 cells treated with empty MNP-PLGA-Lys-Gal and MNP-PLGA-Lys NPs at the same concentration. This may be attributed to the partial release of PTX from the NPs and also reflects that the released PTX still possessed high anticancer activity.

In vitro cell viability of cancer cells has been compared with that of normal CCL-171 cells. The results are presented in Figure 7B. The results suggest that cancer cells display lower cell viability than normal cells, which is pretty much exactly the same as cellular uptake imaging. Cancer cells show better particle uptake, accordingly, should respond with higher growth inhibition compared to normal cells.

Hemolysis Assay In Vitro. When nanoparticles are injected into the bloodstream through a vein, it is crucial to possess a good blood compatibility, including low hemolysis and cytotoxicity.[36,37] The effect of the particulate system on hemolysis depends on the ζ-potential and surface charge of the nanoparticles to some extent, because cationic surfaces are more easily to bind to negatively charged cell membranes and lead to human red blood cells (HRBCs) lysis.[3] In the present work, PTX-MNP-PLGA-Lys-Gal NPs did not give rise to apparent hemolysis reaction in the test concentration scope (Figure 8A, B(a)), and the hemolysis percentage rose merely slightly (0.01∼1.56%) as the NP concentration increased in the range 10−1000 μg/mL. Based on the report from literature,[38] this result was still located within the negligible range (<5%). The ζ-potential measurement of the PTX-MNP-PLGA-Lys-Gal NPs demonstrated a negative ζ-potential of about −13.8 mV at blood pH. The negative ζ-potential is attributed to the presence of a free carboxylic group in the Lys residue, with which there was less opportunity to attack negatively charged HRBCs. Thus, the PTX-MNP-PLGA-Lys-Gal NPs may be safe in vivo applications when administered intravenously below a concentration of 1000 μg/mL.

However, in the case of PTX-MNP-PLGA-Lys NPs, a relatively high hemolysis percentage can be observed. Particularly, the percentage increased significantly over a NPs

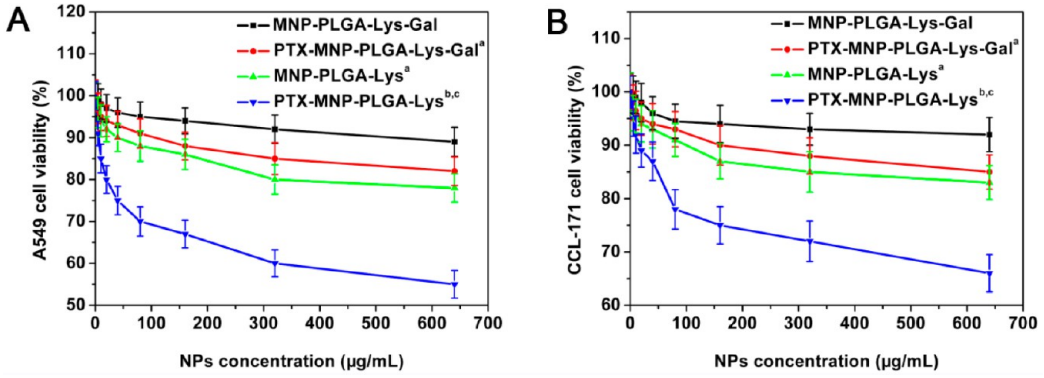

Figure 7. Relative cell viabilities of A549 cells (A) and CCL-171 cells (B) incubated with different NPs (MNP-PLGA-Lys-Gal, PTX-MNP-PLGA-Lys-Gal, MNP-PLGA-Lys, and PTX-MNP-PLGA-Lys) for 24 h. [a]$p < 0.05$ vs MNP-PLGA-Lys-Gal group. [b]$p < 0.05$ vs PTX-MNP-PLGA-Lys-Gal group. [c]$p < 0.05$ vs MNP-PLGA-Lys group.

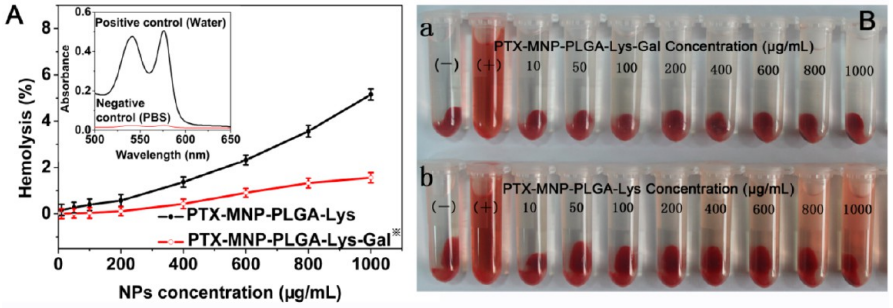

Figure 8. Hemolysis assay in vitro. (A) Hemolysis percentages of PTX-MNP-PLGA-Lys and PTX-MNP-PLGA-Lys-Gal NPs in PBS at concentrations of 10, 50, 100, 200, 400, 600, 800, and 1000 μg/mL. Inset on the top left is absorption spectra of the positive and negative controls. $p < 0.05$ vs PTX-MNP-PLGA-Lys group. (B) Photograph of the hemolysis assay to detect the presence of hemoglobin in the supernatant of HRBCs in PBS at above corresponding NPs concentrations: (a) PTX-MNP-PLGA-Lys-Gal, (b) PTX-MNP-PLGA-Lys.

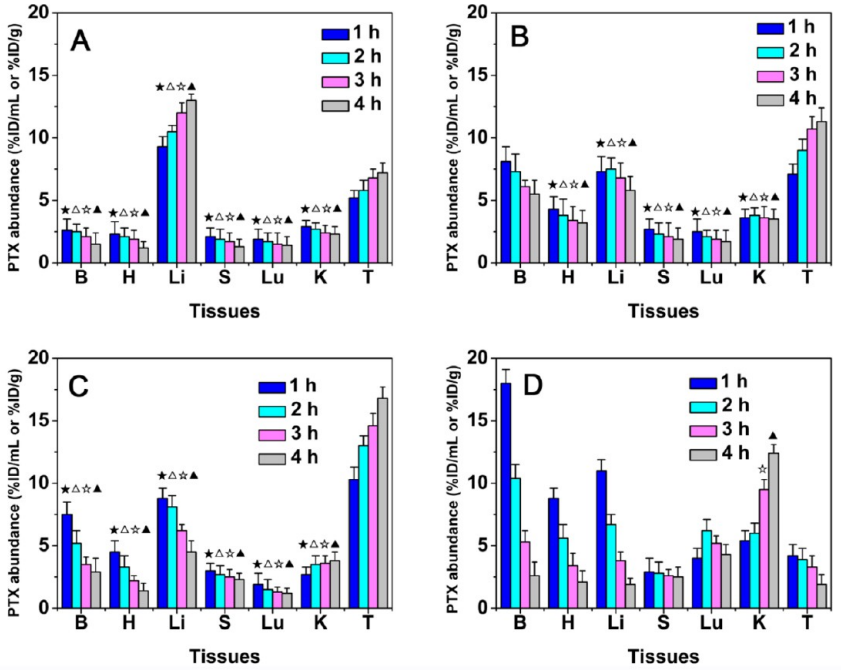

Figure 9. PTX concentration in tissues from tumor-bearing mice treated with (A) PTX-PLGA-Lys-Gal, (B) PTX-MNP-PLGA-Lys, (C) PTX-MNP-PLGA-Lys-Gal NPs, and (D) free PTX. Vertical axis means percent injected dose per milliliter (%ID/mL) of blood or per gram (%ID/g) of tissue. The horizontal axis shows all tissues denoted as B (Blood), H (Heart), Li (Liver), S (Spleen), Lu (Lung), K (Kidney), and T (Tumor). The data are expressed as mean ± SD ($n = 5$). ★ $p < 0.05$ vs tumor tissue (1 h). Δ $p < 0.05$ vs tumor tissue (2 h). ☆ $p < 0.05$ vs tumor tissue (3 h). ▲ $p < 0.05$ vs tumor tissue (4 h).

concentration of 400 μg/mL and reaches 5.15% hemolysis at 1000 μg/mL. From the photographs of HRBCs after exposure to PTX-MNP-PLGA-Lys NPs for 3 h (Figure 8B(b)), it is clearly seen the red hemolysis solution in the range 400−1000 μg/mL. According to the ζ-potential measurement of PTX-MNP-PLGA-Lys NPs, the values displayed a positive ζ-potential of about +16.8 mV, which enhanced electrostatic attraction between NPs and HRBCs and made NPs easier to be uptaken by HRBCs,[39,40] in turn, leading to the hemolysis. Thus, the particle surfaces must show a negative charge off target to avoid nonspecific binding. The pH-sensitive property of surface charge-switched nanoparticles can regulate dynamically particle interactions with target cells and, consequently, reduce nonspecific binding in bloodstream.

Biodistribution Patterns In Vivo. Figure 9 showed distribution status of PTX to the different tissues from mice treated by PTX-PLGA-Lys-Gal, PTX-MNP-PLGA-Lys, and PTX-MNP-PLGA-Lys-Gal NPs and free PTX. It can be found in the PTX-PLGA-Lys-Gal group (Figure 9A) that the highest PTX content emerged in liver > tumor > kidney > blood > heart > lung > spleen. The distribution of PTX to the liver always is the highest within 4 h, which is mainly attributed to the use of galactose, which can lead the liver localization of particles. The distribution of PTX to the tumor was the second of seven tissues, indicating that Lys−Gal part play a role in targeting tumor. However, prominent distribution in the tumor was not found in the absence of magnetomotive, although a magnetic guide was sustained after intravenous injection of NPs.

The PTX content in tumors from PTX-MNP-PLGA-Lys-treated mice (Figure 9B) was obviously higher than that from group A, reflecting that the specific effect is significant under magnetic guiding in vivo though switchable part is imperfect on NPs. Relative to group A, furthermore, the distribution of PTX presented the tendency of slight enhancement in the other five tissues except for liver, which suggested that the binding

capability to normal tissue cells increased when the NPs surface was enclosed by the positively charged Lys residue.

In the PTX-MNP-PLGA-Lys-Gal group (Figure 9C), at the first hour, the highest PTX content was successively in tumor > liver > blood > heart > kidney > spleen > lung. Especially, the concentration of PTX in tumor was significantly ($P < 0.05$) elevated and accounted for 16.8% at 4 h, while the contents of PTX in the heart, blood, and liver were significantly ($P < 0.05$) reduced. This demonstrated the excellent tumor-targeting property of PTX-MNP-PLGA-Lys-Gal NPs under magnetic induction and Lys−Gal triggering. As compared with our recent publication,[29] the present datum was close to that (18.8%) of treatment with cRGD-functionalized polymeric MNPs, reflecting that surface charge switching-triggering targeting was similar to that of cRGD-inducing molecule targeting. It is interesting to replace cRGD peptide with Lys−Gal moiety due to low cost in synthesizing Lys−Gal moiety. Moreover, although the distribution of NPs in the liver was remarkable at 1 h because of the interception of the reticuloendothelium and the affinity of galactose to liver, the effects gradually weakened over time. The distribution amounts of PTX in the lung and spleen did not show significant changes in the process of 4 h magnetic guiding. The concentration of PTX in the kidney only slightly increased during 4 h magnetic induction, suggesting that the absorption and the removal of PTX takes a long time.

In free PTX-treated mice (Figure 9D), PTX distributions were lower to the tumor than to blood, heart, liver, and kidney beside spleen and lung at 1 h, as compared with the PTX-MNP-PLGA-Lys-Gal group. Initially, free PTX was dramatically situated in blood and cardiac muscle at 1 h, which would cause toxic side effects. When the time continued through 4 h, the distribution of PTX to the kidney was significantly ($P < 0.05$) enhanced. On the contrary, PTX concentration in tumor solely accounted for approximately one-ninth of that of group C, indicating more limited tumor uptake when compared to Lys-Gal-modified and MNP-loaded simultaneously NPs.

Tumor Inhibitory Rate. The morphological difference of 180 sarcoma tumors affected by free PTX, PTX-MNP-PLGA-Lys NPs, and PTX-MNP-PLGA-Lys-Gal NPs is shown in Figure 10. Antitumor researches showed that PTX-PLGA-Lys-Gal, PTX-MNP-PLGA-Lys, and PTX-MNP-PLGA-Lys-Gal NPs inhibited the development of tumor at different levels with tumor inhibitory rates of 32.3%, 53.5% and 78.8%, respectively (Table 2). The differences are significant ($P < 0.05$) as compared with the control group. It is found that the tumor inhibition rates were higher in the two MNP-containing groups than in the group without MNPs, and the inhibition rates of PTX-MNP-PLGA-Lys and PTX-MNP-PLGA-Lys-Gal were about 1.7 times and 2.4 times as high as that of PTX-PLGA-Lys-Gal, respectively. In fact, besides targeting NPs to tumor tissue by magnetic guiding, MNPs encapsulated in PLGA NPs can convert irradiation energy into heat under NIR laser beam, causing tumor cell apoptosis because tumor cells are more susceptible to the hyperthermia. At the same, the temperature triggered by magnetic hyperthermia turns on a channel of drug escape because of the degradation of PLGA. The thermosensitive property of nanoparticles contributes to the achievement of controlled release.

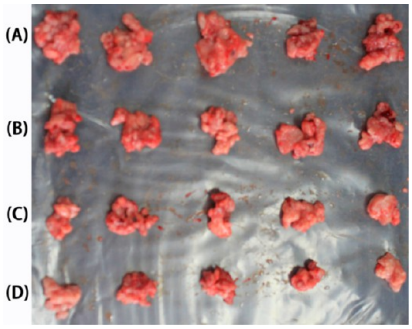

Figure 10. Morphology of tumor tissues from the 180 sarcoma-bearing Balb/c mice treated with magnetic guide and drug-coupled NIR treatment in vivo. (A) Control; (B) PTX-PLGA-Lys-Gal NPs; (C) PTX-MNP-PLGA-Lys NPs; (D) PTX-MNP-PLGA-Lys-Gal NPs.

Table 2. Anticancer Properties of PTX-PLGA-Lys-Gal, PTX-MNP-PLGA-Lys, and PTX-MNP-PLGA-Lys-Gal NPs in Tumor-Bearing Mice[a]

goups	tumor mass (g)	tumor inhibitory rate (%)[b]
control (PBS)	1.70 ± 0.31	
PTX-PLGA-Lys-Gal	1.15 ± 0.14[c]	32.3 ± 3.4
PTX-MNP-PLGA-Lys	0.79 ± 0.14[c]	53.5 ± 4.2
PTX-MNP-PLGA-Lys-Gal	0.36 ± 0.12[c,d]	78.8 ± 5.5[d]

[a]The data are expressed as mean ± S.D ($n = 5$). [b]Tumor inhibitory rate (%) were calculated on the basis of tumor mass. [c]$p < 0.05$ vs control group. [d]$p < 0.05$ vs PTX-PLGA-Lys-Gal group.

Further research showed that, in the case of two MNPs-containing NPs treatment groups (PTX-MNP-PLGA-Lys-Gal and PTX-MNP-PLGA-Lys), the inhibitory effect of tumor in former was better than that in the latter, which can be attributed to surface charge effects. PTX-MNP-PLGA-Lys-Gal NPs present negative charges (ζ potential = −13.8 mV) in near neutral medium, so PTX-MNP-PLGA-Lys-Gal NPs were repelled by negatively charged cell membrane as delivered in bloodstream (pH 7.4). When the NPs were delivered to a tumor site, the pH of the microenvironment decreased from pH 7.4 to approximately pH 5.3, leading to the decomposition of Schiff base modified NPs, followed by protonation of exposed ε-amino groups in lysine residues. Subsequently, the specific binding to tumor was achieved through opposite charges attraction between the positively charged NPs and the negatively charged cell membrane. This pH-switchable property of nanoparticles at targeting site increased the therapeutic effcacy and reduced the drug loss by promoting specific binding to the tumor cells.

CONCLUSIONS

The novel dual signal-responsive paclitaxel-loaded MNP-PLGA-Lys-Gal nanoparticles were synthesized and characterized for the controlled release of anticancer drug. The resulting nanovehicle showed high MNP/drug payload due to the use of the OA-coated MNPs. This particulate system designed for targeting to tumor was capable of switching the surface charge of the PTX-MNP-PLGA-Lys-Gal NPs from anionic above pH 7.0 to cationic below pH 6.5. The cumulative release of PTX from PTX-MNP-PLGA-Lys-Gal NPs could reach 46% within 30 min under NIR irradiation, which was attributed to the presence of thermosensitive material (PLGA) and magnetic hyperthermia. The in vitro cytotoxicity study and cellular uptake assessment concordantly manifested that the deblocking PTX-MNP-PLGA-Lys NPs possessed preferential targeting property to tumor cells. On the contrary, blocking PTX-MNP-PLGA-Lys-Gal NPs revealed the safety during circulation due to its low hemolysis effect. Based on biodistribution and tumor

inhibition data in vivo, the targeting of Lys-Gal-modified polymeric magnetic nanoparticles to tumor was close to that of cRGD-functionalized polymeric MNPs in our recent publication, reflecting that surface charge switching-triggering targeting was similar to cRGD-inducing molecule targeting. This is a highlight for the application in anticancer due to relatively lower cost in synthesizing Lys−Gal moiety than cRGD peptide.

■ ASSOCIATED CONTENT

Supporting Information

Further details of determination of paclitaxel content by RP-HPLC method and degradation rate of the PTX-MNP-PLGA-Lys-Gal nanoparticles. This material is available free of charge via the Internet at http://pubs.acs.org.

■ AUTHOR INFORMATION

Corresponding Author

*Tel.: +86-15117266908. Fax: +86-931-891-5208. E-mail: shenjianmin@lzu.edu.cn.

Notes

The authors declare no competing financial interest.

■ ACKNOWLEDGMENTS

This study was supported by the basic scientific research business expenses of the central university and open project of key laboratory for magnetism and magnetic materials of the ministry of education, Lanzhou University (no. LZUMMM2012006).

■ REFERENCES

(1) Child, H. W.; Pino, P. A.; Fuente, J. M. D. L.; Hursthouse, A. S.; Stirling, D.; Mullen, M.; McPhee, G. M.; Nixon, C.; Jayawarna, V.; Berry, C. C. *ACS Nano* **2011**, *5*, 7910−7919.
(2) Farokhzad, O. C.; Langer, R. *ACS Nano* **2009**, *3*, 16−20.
(3) Shen, Y. Q.; Zhan, Y. H.; Tang, J. B.; Xu, P. S.; Johnson, P. A.; Radosz, M.; Van Kirk, E. A.; Murdoch, W. *AIChE J.* **2008**, *54*, 2979−2989.
(4) Yoo, J. W.; Doshi, N.; Mitragotri, S. *Adv. Drug Delivery Rev.* **2011**, *63*, 1247−1256.
(5) Sankaranarayanan, J.; Mahmoud, E. A.; Kim, G.; Morachis, J. M.; Almutairi, A. *ACS Nano* **2010**, *4*, 5930−5936.
(6) Chen, Y. C.; Liao, L. C.; Lu, P. L.; Lo, C. L.; Tsai, H. C.; Huang, C. Y.; Wei, K. C.; Yen, T. C.; Hsiue, G. H. *Biomaterials* **2012**, *33*, 4576−4588.
(7) Zhao, B. X.; Zhao, Y.; Huang, Y.; Luo, L. M.; Song, P.; Wang, X.; Chen, S.; Yu, K. F.; Zhang, X.; Zhang, Q. *Biomaterials* **2012**, *33*, 2508−2520.
(8) Min, K. H.; Kim, J. H.; Bae, S. M.; Shin, H.; Kim, M. S.; Park, S.; Lee, H.; Park, R. W.; Kim, I. S.; Kim, K. *J. Controlled Release* **2010**, *144*, 259−266.
(9) Oh, K. T.; Kim, D.; You, H. H.; Ahn, Y. S.; Lee, E. S. *Int. J. Pharm.* **2009**, *376*, 134−140.
(10) Kaminskas, L. M.; Kelly, B. D.; McLeod, V. M.; Sberna, G.; Owen, D. J.; Boyd, B. J.; Porter, C. J. H. *J. Controlled Release* **2011**, *152*, 241−248.
(11) Ahmed, N.; Michelin-Jamois, M.; Fessi, H.; Elaissari, A. *Soft Matter* **2012**, *8*, 2554−2564.
(12) Medeiros, S. F.; Santos, A. M.; Fessi, H.; Elaissari, A. *J. Polym. Sci., Polym. Chem.* **2010**, *48*, 3932−3941.
(13) Freichels, H.; Pourcelle, V.; Auzely-Velty, R.; Marchand-Brynaert, J.; Jerome, C. *Biomacromolecules* **2012**, *13*, 760−768.
(14) Mornet, S.; Vasseur, S.; Grasset, F.; Duguet, E. *J. Mater. Chem.* **2004**, *14*, 2161−2175.
(15) Rahman, Md. M.; Elaissari, A. *Sep. Purif. Technol.* **2011**, *81*, 286−294.
(16) Medeiros, S. F.; Santos, A. M.; Fessi, H.; Elaissari, A. *Int. J. Pharm.* **2011**, *403*, 139−161.
(17) Fan, Z.; Shelton, M.; Singh, A. K.; Senapati, D.; Khan, S. A.; Ray, P. C. *ACS Nano* **2012**, *6*, 1065−1073.
(18) Hilger, I.; Fruhauf, K.; Andra, W.; Hiergeist, R.; Hergt, R.; Kaiser, W. A. *Acad. Radiol.* **2002**, *9*, 198−202.
(19) Avgoustakis, K.; Beletsi, A.; Panagi, Z.; Klepetsanis, P.; Karydas, A. G.; Ithakissios, D. S. *J. Controlled Release* **2002**, *79*, 123−135.
(20) Zhang, J. L.; Srivastava, R. S.; Misra, R. D. K. *Langmuir* **2007**, *23*, 6342−6351.
(21) Overgaard, K.; Overgaard, J. *Eur. J. Cancer* **1972**, *8* (1), 65−68.
(22) Huang, H. C.; Barua, S.; Sharma, G.; Dey, S. K.; Rege, K. *J. Controlled Release* **2011**, *155* (3), 344−357.
(23) Yanase, S.; Nomura, J.; Matsumura, Y.; Kato, H.; Tagawa, T. *Photodiagn. Photodyn. Ther.* **2012**, *9* (4), 369−375.
(24) Dilnawaz, F.; Singh, A.; Mohanty, C.; Sahoo, S. K. *Biomaterials* **2010**, *31*, 3694−3706.
(25) Singh, A.; Dilnawaz, F.; Mewar, S.; Sharma, U.; Jagannathan, N. R.; Sahoo, S. K. *ACS Appl. Mater. Interfaces* **2011**, *3*, 842−856.
(26) Harikrishnan, S.; Kalaiselvam, S. *Thermochim. Acta* **2012**, *533*, 46−55.
(27) Shen, J. M.; Xu, L.; Lu, Y.; Cao, H. M.; Xu, Z. G.; Chen, T.; Zhang, H. X. *Int. J. Pharm.* **2012**, *427*, 400−409.
(28) Liu, X. Q.; Kaminski, M. D.; Chen, H. T.; Torno, M.; Taylor, L. T.; Rosengart, A. J. *J. Controlled Release* **2007**, *119*, 52−58.
(29) Shen, J. M.; Gao, F. Y.; Yin, T.; Zhang, H. X.; Ma, M.; Yang, Y. J.; Yue, F. *Pharmacol. Res.* **2013**, *70* (1), 102−115.
(30) Chen, C.; Hong, L.; Xu, Z. Q.; Liu, L.; Wang, R. *Org. Lett.* **2006**, *8*, 2277−2280.
(31) Shen, J. M.; Guan, X. M.; Liu, X. Y.; Lan, J. F.; Cheng, T.; Zhang, H. X. *Bioconjugate Chem.* **2012**, *23*, 1010−1021.
(32) Liu, P. F.; Wang, H. Z.; Li, Y. G.; Duan, Y. R. *J. Macromol. Sci. Part A* **2009**, *46*, 1024−1029.
(33) Guo, M.; Su, X. Y.; Kong, L.; Li, X.; Zou, H. F. *Anal. Chim. Acta* **2006**, *556*, 183−188.
(34) Bulte, J. W. M.; Brooks, R. A.; Moskowitz, B. M. *Magnet. Reson. Med.* **1999**, *42*, 379−384.
(35) Du, Y. F.; Chen, W.; Zheng, M.; Meng, F. H.; Zhong, Z. Y. *Biomaterials* **2012**, *33*, 7291−7299.
(36) Lin, Y. S.; Haynes, C. L. *J. Am. Chem. Soc.* **2010**, *132*, 4834−4842.
(37) Wu, H. X.; Zhang, S. J.; Zhang, J. M.; Liu, G.; Shi, J. L.; Zhang, L. X.; Cui, X. Z.; Ruan, M. L.; He, Q. J.; Bu, W. B. *Adv. Funct. Mater.* **2011**, *21*, 1850−1862.
(38) Sun, Y. N.; Wang, C. D.; Zhang, X. M.; Ren, L.; Tian, X. H. *J. Nanosci. Nanotechnol.* **2011**, *11*, 1210−1216.
(39) Avgoustakis, K. *Curr. Drug Delivery* **2004**, *1*, 321−333.
(40) Mansouri, S.; Cuie, Y.; Winnik, F.; Shi, Q.; Lavigne, P.; Benderdour, M. *Biomaterials* **2006**, *27*, 2060−2065.